High-Bandwidth Graded-Index Polymer Optical Fiber

Yasuhiro Koike, Takaaki Ishigure, and Eisuke Nihei

(Invited Paper)

Abstract—**High-bandwidth (2 GHz · km) Graded-Index Polymer Optical fiber (GI POF) was successfully obtained by the new interfacial-gel polymerization technique in which the unreactive component was used in order to obtain the quadratic refractive-index distribution. This high-bandwidth GI POF makes it possible to transmit high-speed optical signals in the short range network which was not covered by the Step-Index type POF commercially available. The high bandwidth GI POF will open the way for great advantages in the high-speed multimedia network.**

I. Introduction

REALIZATION of the all optical subscriber system has gained more and more interest so far with the development of fiber optic technology. Single-mode silica optical fibers have been widely used as long-distance and high-speed communication media because of their excellent transparency and because it makes possible to obtain the necessary precise control of the core diameter. However, inorganic glasses are not a universally ideal material especially for fiber connection and handling problems. The small core of the single mode fiber requires high accuracy in the fiber connection, which increases the cost of the whole system. Moreover, when the single mode fiber is connected to the light source such as laser diode, a more complicated lens system is required for high coupling efficiency. With the spread of fiber-optic technology, new materials have been required to provide the needed properties in practical optical systems.

Recently, there has been considerable interest in the development of a polymer optical fiber (POF) [1]–[7]. Although the transmission attenuation is relatively large (20–300 dB/km) due to the organic molecular structure, it is possible to use the inexpensive POF in the short range communication area within 200 m, namely in a building, home, and termination area of "Fiber to the home (FTTH)." In such short distance communications, many junctions and connections of optical fibers would be necessary. The POF with a large core diameter (such as 0.5 mm or more) is one of the promising candidates to solve the serious problem in splicing the single mode optical fiber owing to its small core diameter (5–10 μm). The large core of the POF would make it possible to adopt injection molding polymer connectors, which dramatically decreases the total cost of the system.

Manuscript received September 1, 1994; revised January 18, 1995.

The authors are with Faculty of Science and Technology, Keio University, 3-14-1, Hiyoshi, Kohoku-ku, Yokohama 223, Japan.

IEEE Log Number 9411026.

However, all commercially available POF's have been of the step-index (SI) type whose bandwidth of transmission is limited to about 5 MHz · km [8] due to modal dispersion. Therefore, even in the short range communication area, the SI POF will not be able to cover the data rate of more than 100 Mb/s that will be necessary in fiber distributed data interface (FDDI) [9], synchronous digital hierarchy (SDH) [10], and broadband integrated services digital network (B-ISDN) [11] etc. standards of the telecommunication area. The SI POF has been competitive with conventional twisted pair or coaxial cables in bandwidth, and has not been able to find the advantageous discrimination from them. The narrow bandwidth of SI POF has confined the use of POF only to light guides and illumination components so far.

The key element for POF to go into the data transmission media would be, we believe, the large core graded-index (GI) POF that combines an intrinsic high bandwidth. Very recently, the large core GI POF whose bandwidth was about 2 GHz · km was successfully prepared for the first time at Keio University [12]. The bandwidth of the GI POF is about 400 times larger than that of any conventional SI POF's, which will cover the bandwidths of any attractive high-speed multimedia inside the customer premises.

In this paper, the birth of the GI POF is reviewed, and the preparation methods and the transmission properties such as bandwidth and attenuation etc. are described in detail. We propose a new concept of high-speed multimedia network by the large core GI POF.

II. Fiber Classes

The POF developed so far has been divided into two classes of structure: one is of step-index (SI) and the other is of graded-index (GI).

In the case of the SI POF [13], [14] which has a core region and a cladding as shown in Fig. 1(a), as light is transmitted by reflecting at the boundary of core and cladding, an impulse injected into the fiber is spread over a time interval that is equal to the difference of the arrival times of the slowest and fastest modes. After the pulses have traveled a certain distance, this spreading causes them to overlap to such an extent that the information which they contain scrambled. Therefore, the SI POF is aimed at low data-rate transmission, image guide, and illumination. Fig. 1(a) shows the real data of input and spread output pulses for the SI POF with 15-m length.

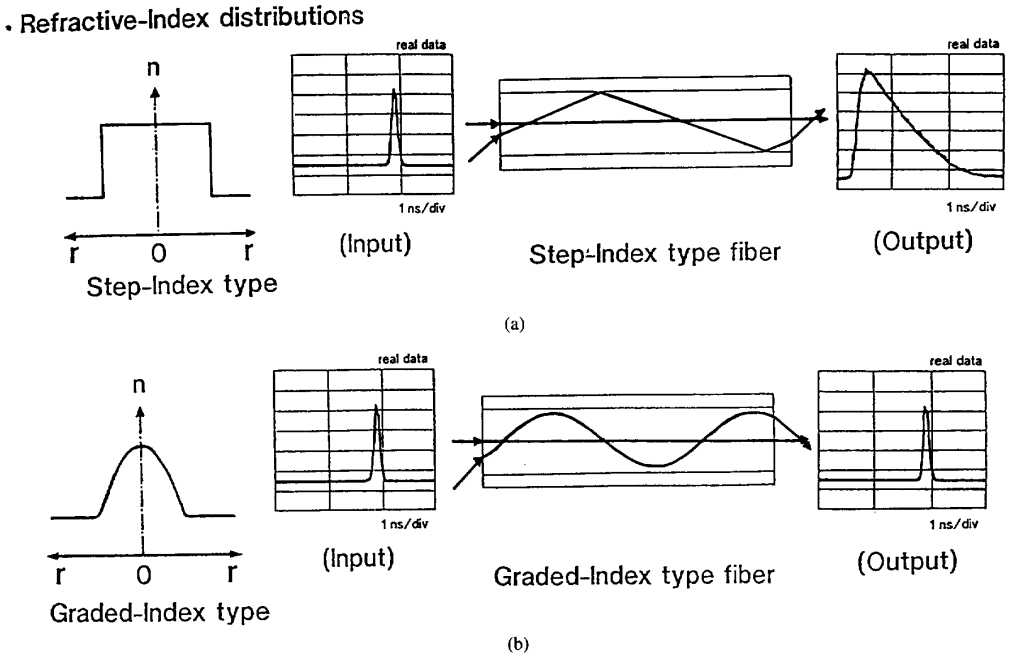

Fig. 1. Schematic representation of light transmission through SI and GI POF's.

Usually, poly(methyl methacrylate) (PMMA) is used as the core material and fluoropolymer as the cladding material. In this case, the refractive index difference between core and cladding comes to about 0.1, resulting in the high numerical aperture (NA). Here, the numerical aperture is defined as follows

$$\mathrm{NA} = (n_{\mathrm{core}}^2 - n_{\mathrm{cladd}}^2)^{\frac{1}{2}} = \sin\left(\frac{\theta_A}{2}\right) \tag{1}$$

where n_{core} and n_{cladd} represent the refractive indices of the core and cladding, respectively, and θ_A corresponds to the acceptance angle. Typical POF has an NA of about 0.5, that offers 60° of an acceptance angle, compared with 0.14 and 16°, respectively, for a glass fiber.

Regarding the GI POF, a remedy for the pulse broadening problem in SI POF can be found by constructing a refractive-index distribution which is a parabolic form in the fiber core. The reason why this type of the fiber exhibits less pulse broadening can be understood in the following way. As in the case of GI POF, the shortest ray path follows the fiber axis, while longer ray paths oscillate around the ray axis as shown in Fig. 1(b). However, along most of the oscillating ray path, the refractive-index is smaller than that on the fiber axis. As the velocity of light is inversely proportional to the refractive-index n, the light that travels along the oscillating paths travels at a higher speed than the light that follows the axis. This greater speed partially compensates for the longer distance traveled. This result suggests that transit times for the oscillating ray paths are not very different from the transit time for the axial ray path. Since the pulse broadening is proportional to the maximum difference in transit times, small pulse broadening is expected of the GI POF.

The history of POF development for both SI and GI POF's are summarized in Table I. The POF of SI type was developed at Du Pont for the first time by using PMMA as the core material and fluoropolymer as the cladding material [15]. Throughout the 1970's, Nippon Telegraph and Telephone (NTT) [16]–[18] and Mitsubishi Rayon [19] have worked on the improvement in the attenuation of the POF by adopting the extrusion method based on the Du Pont's method. In 1983, Kaino *et al.* reported that [20] low-loss POF with 20 dB/km attenuation was achieved by using the all deuterated PMMA (PMMA-d8). All of them have been of the SI type. The first GI POF was reported from Keio University [21] in 1982. Since the GI POF at that time was prepared by utilizing the monomer reactivity ratio, the excess scattering loss due to the phase separation of the copolymer increased the total attenuation up to 1000 dB/km, which was about ten times larger than that of the SI POF. Development of the interfacial-gel polymerization technique enabled the dramatic reduction in the total attenuation of the GI POF. Further, the high bandwidth of 2 GHz · km which was about 400 times larger than that of the conventional SI POF was experimentally recognized by using 55-m length GI POF [12].

III. Preparation of GI POF

A. Formation of Graded-Index

First, a polymer tube which composes the cladding of the fiber was prepared by MMA monomer as follows: a glass tube in which the MMA monomer mixture with polymerization initiator and chain transfer agent was placed, was rotated on its axis at approximately 3000 r.p.m. in the oven at 70°C.

TABLE I
POF DEVELOPMENT. PMMA: POLY METHYLMETHACRYLATE; PST: POLY STYRENE; PMMA-D8: DEUTERATED PMMA; PC: POLY CARBONATE; P5F3DST: PENTAFLUOROTRIDEUTEROSTYRENE; MMA CO VPAC: COPOLYMER OF MMA AND VINYL PHENYL ACETATE; MMA CO VB: COPOLYMER OF MMA AND VINYL BENZOATE

Organization	Core Material	Cladding Material	Classification	Minimum Attenuation (dB/km)	Wavelength (nm)	Year	Comment
Du Pont	PMMA	Fluoro-polymer	SI	500	650	1968	
Toray	PS	PMMA	SI	1100	670	1972	
Du Pont	PMMA-d8		SI	180	790	1977	For near-IR
Mitsubishi Rayon	PMMA	Fluoro-polymer	SI	300	650	1978	
NTT	PMMA	Fluoro-polymer	SI	55	568	1982	
NTT	PS		SI	114	670	1982	
Keio University	MMA co VPAc	PMMA	GI	1070	670	1982	
NTT	PMMA-d8		SI	20	650	1983	
Mitsubishi Rayon	PMMA	Fluoro-polymer	SI	110	570	1983	
Asahi Chemmical	PMMA	Fluoro-polymer	SI	80	570	1985	
Fujitsu	PC	poly olefin	SI	450	770	1986	Highly thermal resistant
NTT	P(5F3DSt)	Fluoro-polymer	SI	178	850	1986	For nea-IR
Hitachi	Thermoset resin	Fluoro-polymer	SI	600	650	1987	Highly thermal resistant
Keio University	MMA co VB	PMMA	GI	130	650	1990	
Hoechst Celanese	PMMA	Fluoro-polymer	SI	130	650	1991	
Keio University	PMMA-d8	PMMA-d8	GI	56	688	1992	High-bandwidth (2GHz·km)
Bridgestone	silicone	silicone	SI	800	650	1993	

TABLE II
PROPERTIES OF USED MONOMER AND UNREACTIVE COMPONENTS

Materials	Molecular weight	Volume (Å^3)	Calculated Solubility Parameter (cal/cm^3)$^{1/2}$
MMA	100.1	105.0	7.814(monomer) 9.327 (polymer)
BB	157.0	109.0	8.468
BBP	312.4	305.2	9.599
BEN	212.3	208.7	9.642
DPP	318.3	294.4	9.094

The MMA monomer in the glass tube was placed on the inner wall of the tube due to centrifugal force, and polymerized with maintaining the shape. The resultant polymer became a tube which was used as a container for the polymerization of the core region. Next, the polymerization process of the core was performed as follows: the PMMA tube was filled with MMA monomer mixture with polymerization initiator, the chain transfer agent, and another organic compound (M_2 dopant) which had a higher refractive index than that of PMMA. The M_2 dopant compounds used in this paper are bromobenzen (BB), benzyl butyl phthalate (BBP), benzyl benzoate (BEN), and diphenyl phthalate (DPP) whose properties are shown in Table II. The PMMA tube filled with the monomer mixture was horizontally placed in an oven at 95°C and was rotated on its axis at approximately 50 r.p.m. for 24 hours. Here, the inner wall of the polymer tube is slightly swollen to the monomer mixture and a gel phase is formed on the inner wall of the tube. It is well known that the reaction of the polymerization is accelerated in the gel state due to so-called "gel-effect." Therefore, the polymer phase is gradually formed from the gel phase on the inner wall of the tube, including a large amount of remaining monomer. The thickness of the polymer phase gradually increases, and finally the polymer phase reaches up to the center axis of the tube.

During this polymerization process, the radial graded-index distribution is formed by the following mechanism: This process is schematically shown in Fig. 2. In Fig. 2(a), the closed and open circles signify MMA and the M_2 dopant molecules, respectively. Since the aromatic compound whose molecular volume was larger than that of MMA monomer molecule was used as the M_2 dopant, MMA molecules can more easily diffuse into the polymer phase than the M_2 dopants. This selective diffusion process is shown in Fig. 2(b). Therefore, the M_2 dopant molecules are gradually concentrated in the center region as the thickness of the polymer phase increases. Finally the polymer phase reaches the center axis of the tube and the radial distribution of the M_2 dopant concentration is formed as shown in Fig. 2(c). Since the refractive index of the M_2 dopant is higher than that of PMMA, the refractive index distribution in which the refractive index decreases monotonically from the center axis of the core to the periphery is obtained. After that, the heat-treatment was carried

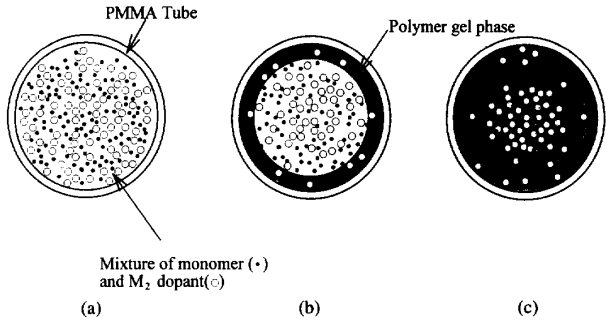

Fig. 2. Schematic representation of the selective diffusion of monomer and M_2 dopant molecules into polymer gel phase to form the graded-index distribution.

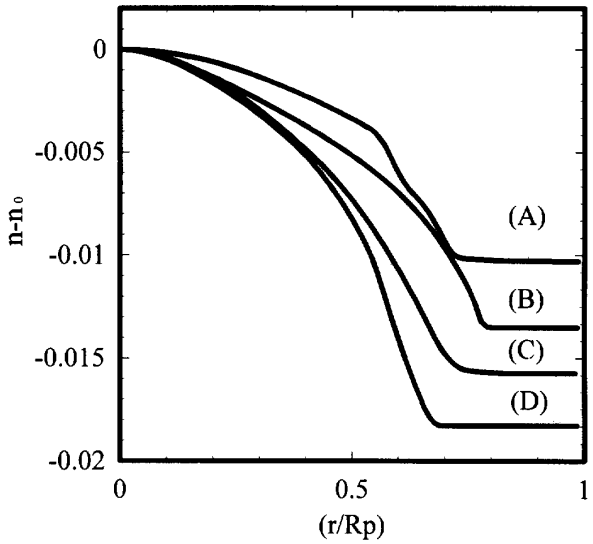

Fig. 3. Refractive-index distribution of the MMA-M_2 dopant system GI preform. (a) MMA-BB system. (b) MMA-BEN system. (c) MMA-BBP system. (d) MMA-DPP system. Rp: Radius.

out at 110°C for 24 hours under 0.2 mmHg to complete the polymerization.

B. Fiber Fabrication

The GI POF was obtained by heat-drawing of GI preform at 160°C–230°C. The GI POF with a desired diameter was obtained by controlling the velocity of taking up the fiber. In this paper, the fiber diameter was 0.5 mm.

C. Refractive-Index Distribution

The refractive-index distribution of the preform was measured by the longitudinal interferometric technique [22]. As shown in Fig. 3, all preforms prepared from various dopants systems have almost quadratic index profiles, where n_0 means the refractive index at the center of the core and R_p is the radius of the preform.

The reproducibility of the refractive index distribution of the MMA-BBP system preform (MMA/BBP= 5/1 (wt. /wt.)) is

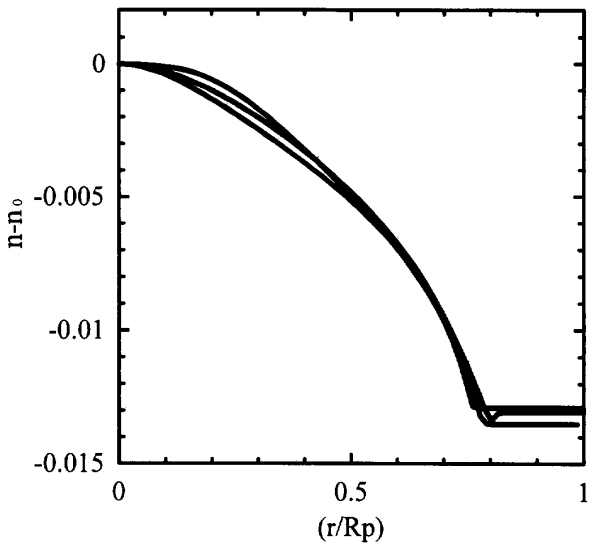

Fig. 4. Reproducibility of the refractive-index profile of MMA-BBP system GI preform.

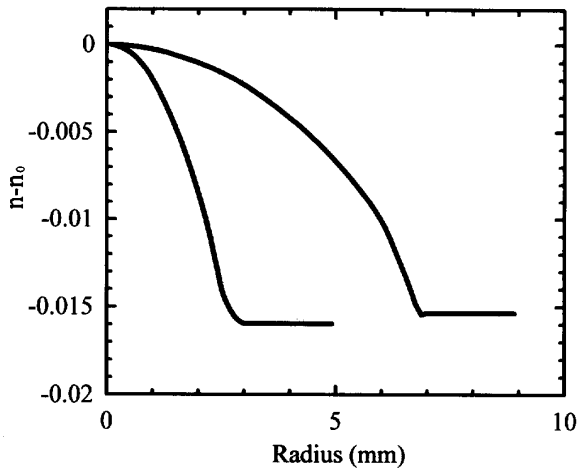

Fig. 5. Refractive-index profile of MMA-BEN system GI preform with 18-mm diameter compared with the profile with 10-mm diameter.

shown in Fig. 4. The diameters of all preforms were 10 mm. It is confirmed that almost the same refractive index distributions can be obtained when the polymerization condition is the same, since the interfacial-gel polymerization is very simple in principle and no external influence during the polymerization must be added.

Fig. 5 shows the refractive-index distributions of the preforms having 10 mm and 18 mm diameters. Fiber length possibly obtained from a preform depends on the preform diameter and length. It was experimentally confirmed that the quadratic refractive index distribution was successfully obtained even in the case of such a large diameter (18 mm) preform.

The optimum refractive index distribution formed in the preform should be stably maintained even after the heat-

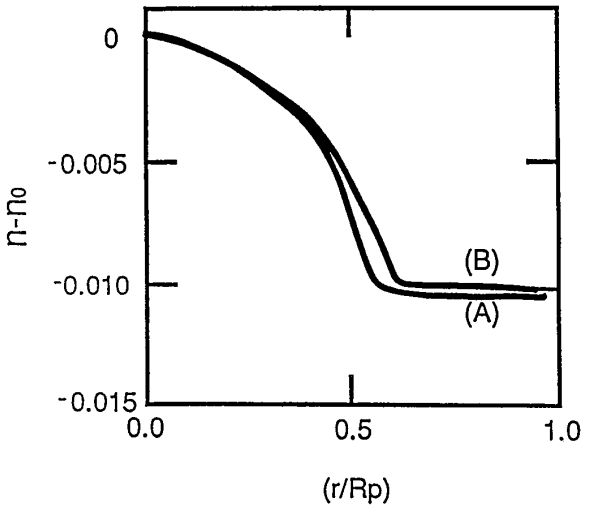

Fig. 6. Refractive-index distribution of MMA-BBP system GI preform and resulting GI POF. (A) Fiber (0.5 mm)-diameter. (B) Preform (16 mm)-diameter.

drawing process to keep the high bandwidth. Fig. 6 shows the comparison of the refractive index profiles between the preform and the resulting fiber. The diameters of the preform and fiber were 16 mm and 0.5 mm, respectively. It is confirmed that the refractive index profiles can be maintained throughout the fiber fabrication process. The numerical apertures (NA) of the MMA-BBP system GI POF estimated from the index difference shown in Fig. 6 is about 0.21.

The graded-index materials mentioned above are applicable not only to the communication grade fiber but also to a graded-index rod lens. In the conventional materials for designing lenses, focusing and imaging properties are determined by varying the curvature because the refractive-index is homogeneous. In contrast, in the radial graded-index rod the light beam is gradually bent inside the material according to the index distribution, and goes through a sinusoidal trajectory as shown in Fig. 1(b). Therefore, the graded-index material works as a lens even if both rod surfaces are flat. Fig. 7 shows the clear reversed real image formed on the surface of MMA-BEN system preform. The preform was cut at the position of one fourth (so-called quarter pitch length) of the period of sinusoidal trajectory, and both ends were polished to be optically flat. The lens function of the graded-index rod is described in detail elsewhere [23]–[25]. The diameter of the rod is 16 mm, which is much larger than that of the conventional rod lens (1 ~ 2 mm) prepared by the inorganic glasses such as SELFOC (registered trade name of Nippon Sheet Glass Co.). It is noted that such a large rod lens cannot be easily prepared by the ion-exchange process [26], [27] for inorganic materials.

IV. Bandwidth

The bandwidth measurement of the GI and SI POF's was performed by determining the impulse response of the fiber. The procedure in time domain measurement involves generating and launching very short pulses of light into a sample and then detecting and recording the distorted pulses at the output of the fiber. The experimental set up of this impulse response function measurement is shown in Fig. 8. A pulse of 10 MHz from an InGaAlP laser diode (wavelength = 670 nm) was injected (NA = 0.5.) into the POF. The output pulse was detected by a sampling head (model OOS-01, Hamamatsu Photonics Co.).

The output pulse from the MMA-BBP GI POF whose refractive-index distribution was in Fig. 6 is shown in Fig. 9(b) compared with (a) of the SI POF commercially available. The fiber lengths of both GI and SI POF's were 100 m. It is quite noteworthy that, although the output pulse through the

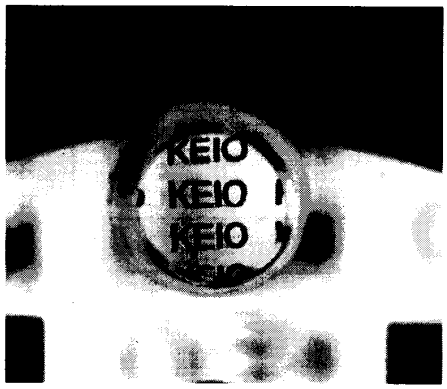

Fig. 7. Photograph of the reversed real image formed on the surface of the quarter pitch length MMA-BEN system GI preform. Diameter: 16 mm.

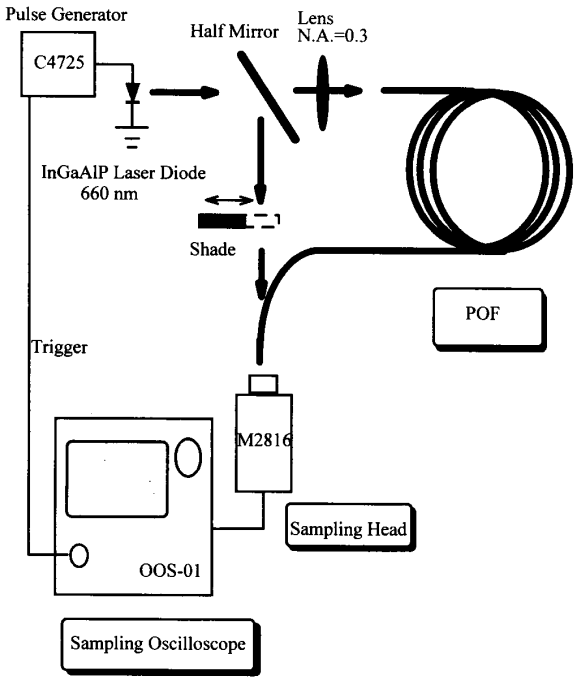

Fig. 8. Schematic representation of the impulse response function measurement.

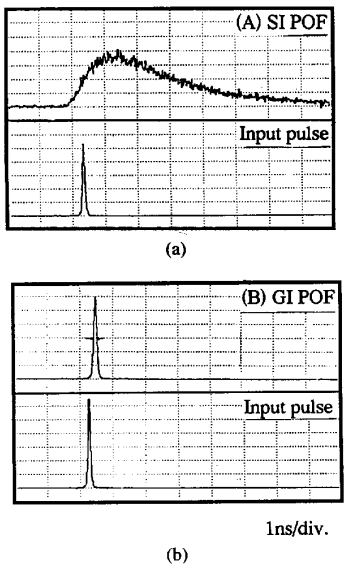

Fig. 9. Pulse spread through GI and SI POF's. Fiber length: 100 m.

SI POF is quite dispersed, the pulse through the GI POF is almost the same as the input pulse even after a 100 m signal transmission. From the input and output pulses, the transfer function of the fiber from which 3 dB optical bandwidth was obtained was estimated by Fourier transform The bandwidth of the conventional SI POF is about 5 MHz · k} while that of the GI POF in Fig. 9 is 2.0 GHz · km, 400 times larger than that of the SI POF.

The bandwidth of the multimode fiber largely depends on the launch condition. It was reported that [28] the SI POF measured with collimated input (NA = 0.01) displays a substantially greater bandwidth than the one measured with a high NA (NA = 0.65) launch condition. In the case of the GI POF, the bandwidth measured with low NA (0.01 ~ 0.1) launch is also greater than that with high NA (0.5) launch. When the launch NA is larger than the NA estimated from the refractive-index distribution of the GI POF, the bandwidth was independent of the launch NA condition because higher modes than the NA of the GI POF were scattered out during transmission. The result in Fig. 9 is in this case. On the other hand, when the launch NA was 0.1 which was smaller than the NA (= 0.2) of the GI POF, the bandwidth of the GI POF was beyond the detection limit of the measurement system. Therefore, in this paper, the launch NA was set to be 0.5 which was higher than the numerical aperture of the GI POF. This may provide reliable and practical data when considering its real use.

It is well known that the bandwidth can be maximized by optimizing the shape of the graded-index distribution of the fiber core. When the index distribution is expressed by a power law of the form

$$n(r) = n_1[1 - 2(r/R)^g\Delta]^{\frac{1}{2}} \tag{2}$$

where the parameter g is the exponent of the power law, and

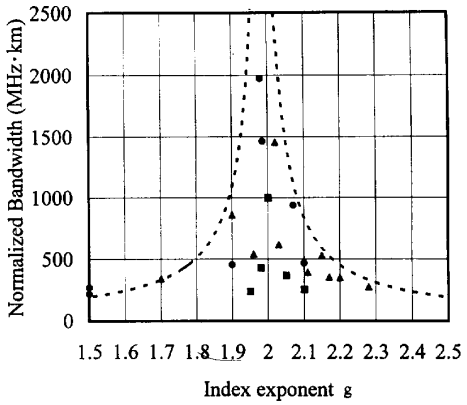

Fig. 10. Bandwidth of GI POF's against the index exponent g. (•): MMA-BBP system GI POF (■): MMA-BB system GI POF (▲): MMA-BEN system GI POF: (- - - -). Calculated bandwidth of the GI POF.

R is core diameter, the bandwidth is maximized [29] when

$$g = g_{\text{opt}} = 2 + \varepsilon - \Delta\frac{(4+\varepsilon)(3+\varepsilon)}{5+2\varepsilon}$$
$$\Delta = \frac{n_0 - n_1}{n_0} \tag{3}$$

where ε is the parameter of the material dispersion, n_0 and n_1 are the refractive indices of the core center and cladding, respectively. Without the material dispersion, it becomes simply

$$g_{\text{opt}} = 2 - \frac{12}{5}\Delta. \tag{4}$$

Since the Δ = 0.01-0.02 for the GI POF in this paper, the maximum bandwidth is achieved when g is about 2. In Fig.10, the bandwidths of the various GI POF's are plotted against the index exponent g by using a least-square technique for (2). Here, the index exponent was estimated by the measured index profile. The bandwidth was normalized for Δ = 0.01.

The bandwidth of the GI POF which has the index profile written by (2) was theoretically estimated by using Gloge's method [30] as follows. The propagation constant may be expressed as

$$\beta = \frac{n_0}{\lambda}\left[1 - 2\Delta\left(\frac{M(\beta)}{N}\right)^{\frac{g}{g+2}}\right]^{\frac{1}{2}} \tag{5}$$

where λ is wavelength and $M(\beta)$ is the cumulative number of transmitted modes with a propagation constant larger than β, which means $M(\beta)$ includes all modes from that of the lowest order (with largest propagation constant) to the mode whose propagation constant is β. The parameter N in (5) is defined as

$$N = \frac{g}{g+2}R^2\frac{{n_0}^2}{\lambda^2}\Delta \tag{6}$$

and gives the total number of guided modes.

By differentiation of (6) the time delay τ written by (7) can be obtained.

$$\frac{\tau}{L} = \frac{d\beta}{d\omega} \tag{7}$$

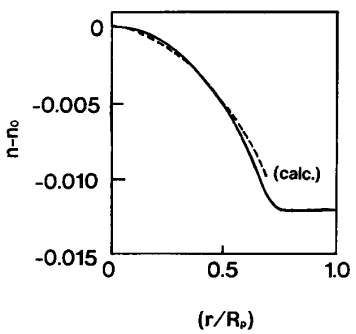

Fig. 11. Refractive-index distribution of the MMA-BB system GI POF (solid curve) in which the bandwidth is 1 GHz · km, and the index distribution (dashed curve) approximated by (2) having g of 2.08. Rp: Radius.

$$\tau = \frac{n_0}{c}\left[\frac{g-2}{g+2}\Delta + \frac{3g-2}{g+2}\frac{\Delta^2}{2}\right]. \tag{8}$$

Then, the pulse spreading through the GI POF was estimated by (8). Finally, the broken curve in Fig. 10 was derived by Fourier transform of the output pulse whose shape was assumed to be a Gaussian impulse.

The bandwidth is maximized around $g = 2$ for the MMA-BBP fiber as predicted in (4) and was 2 GHz · km as shown in Fig. 10. Fig. 11 shows the refractive index distribution of MMA-BB system GI POF (solid curve) whose bandwidth was 1 GHz · km [3]. The broken curve in Fig. 11 was the index profile approximated by (2) using a least-square technique. The index exponent g of the GI POF used in the calculation was $g = 2.08$.

The high bandwidth of the GI POF compared with the conventional SI POF was experimentally confirmed even for a short-distance communication as 50 m-length.

V. Attenuation of Light Transmission

A. Attenuation of GI POF

The intrinsic attenuation of the GI POF is classified into four separate loss mechanisms: a) electronic transition absorption; b) carbon-hydrogen (C-H) vibrational absorption; and c) intrinsic scattering due to both large-size heterogeneities and thermal density fluctuation. The attenuation caused by both intrinsic scattering and electronic transition absorption decreases with increasing wavelength, while the C-H vibrational absorption abruptly increases from about 600 nm wavelength to the infrared region.

The total attenuation spectrum of the GI POF was measured by the cut-back method and by using a spectrum analyzer (ADVANTEST Co. Model TQ8345). Fig. 12 shows the total attenuation spectra of the GI POF's, where the curves (A), (B), and (C) denote the spectra of MMA-BBP, MMA-BEN, and MMA-BB system GI POF's, respectively. It is noted that the total attenuation of the GI POF's at 650-nm wavelength are almost the same as or superior to that of the SI POF commercially available (100–300 dB/km). A more quantitative analysis of the intrinsic loss mechanisms is described below.

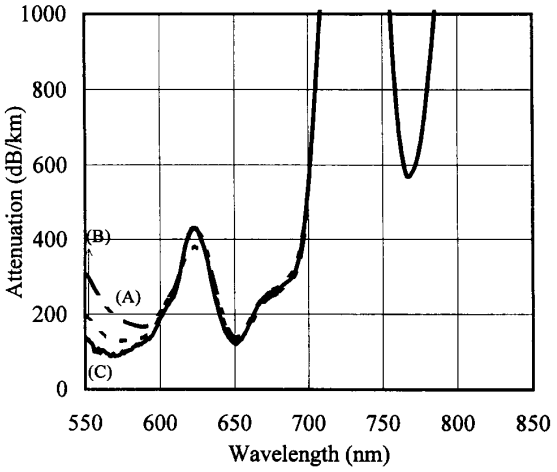

Fig. 12. Total attenuation spectra of GI POF's. (A) MMA-BBP system, (B) MMA-BEN system, (C) MMA-BB system.

B. Absorption Loss

1) Electronic Transition Absorption: The mechanism responsible for the electronic transition absorption depends on transitions between electronic energy levels of the bonds within the materials: the absorption of a photon causes an upward transition, leading to an excitation of the electronic state of the solid. In the case of PMMA, the most significant absorption is caused by the transition of the n-orbital to the π^* orbital of the double bond of carbon-oxygen (C=O) within the polymer molecule. On the other hand, in the case of the poly(styrene) which is also a universal polymer for the POF, as a benzene ring is contained in the monomer unit, the electronic transition absorption loss due to the π to π^* transitions of the double bond of carbon-carbon (C=C) increases and the delocalized bonds of the benzene ring produce an intense absorption in the UV region. It was reported that [18] the effect of the electronic transition absorption on the attenuation at 570 $\sim$ 650-nm wavelength region is obeyed by Urbach's rule [31]. The attenuation due to the electronic transition absorption in poly(styrene) is approximately 100 dB/km at 500-nm wavelength and 7 dB/km at 600 nm, whereas in PMMA it is below 1 dB/km above 500 nm [18]. In considering the attenuation of the GI POF, electronic transition absorption loss should be taken into account because the used dopant has benzene rings in it. However, from the attenuation spectra in Fig. 12, the effect of the electronic transition absorption loss is so small that the attenuation at 650-nm wavelength is independent of the kind of dopant molecules.

2) Carbon-Hydrogen Vibrational Absorption: Although the total attenuation limit for PMMA-core POF reported by Kaino *et al.* [18] is as small as 35 dB/km at a wavelength of 568 nm, the preferred high-power laser diodes (LD's) are available at 650 nm, 780 nm, and longer wavelengths. A serious problem in the PMMA-core POF at these wavelengths is large attenuation due to the absorption loss by high harmonics of carbon-hydrogen vibration (C-H overtone) in the polymer molecule. To solve this problem Sheleinitz at Du

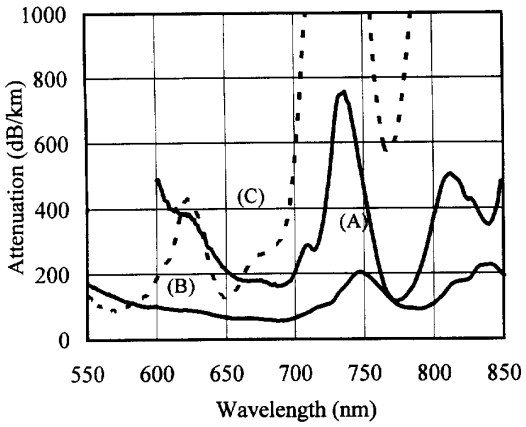

Fig. 13. Total attenuation spectra of the PMMA-d8 base GI POF and fluorinated polymer base GI POF compared with the PMMA-base GI POF. (A) Fluorinated polymer base GI POF. (B) PMMA-d8 base GI POF. (C) PMMA-base GI POF.

Pont proposed an all-deuterated PMMA (PMMA-d8) in 1977 [15], in which the carbon-deuterium (C-D) overtone bands are shifted to longer wavelengths.

A more quantitative estimation of the vibrational absorption loss is made by using the Morse Potential theory [32] described as follows. The energy level, $G(v)$, belonging to the vibrational absorption between two atoms can be written as

$$G(v) = \nu_0(v + 1/2) - \nu_0\chi(v + 1/2)^2 \tag{9}$$

where $v = 1, 2, 3 \cdots$ is the quantum number, χ the anharmonicity constant, and ν_0 the original vibration between only two atoms written as

$$\nu_0 = \frac{\sqrt{\frac{K}{\mu}}}{2\pi c}. \tag{10}$$

K, μ, and c mean the force constant, reduced mass and velocity of light in vacuum, respectively. Then the vth harmonic vibration, ν_v, becomes

$$\nu_v = \frac{\nu_1 v - \nu_1\chi v(v+1)}{1 - 2\chi}. \tag{11}$$

Here, ν_1 denotes the fundamental vibration in real polymer and $\nu_1 = \nu_0$ when $\chi = 0$. From infrared spectroscopic data, one can find ν_1 and ν_2 for all interesting vibration such as C-H and C-D, from which the χ value can be calculated. As for C-H and C-D vibrations, χ is 1.9×10^{-2} and 1.5×10^{-2}, respectively. From the literature [32], the fundamental vibrations ν_1 of C-H, C-D, and carbon-fluorine (C-F) bonds in real polymer exist at 3390, 4484, and 8000-nm wavelength, respectively. Deuterium and halogen atoms are considered to be promising alternatives to shift the wavelength of the fundamental vibration to longer wavelengths than that of a C-H bond. The absorption loss in the polymer due to the overtone intensity is approximated by [32],

$$D_{\max}(\nu_v^{\mathrm{C-X}}) = 3.2 \times 10^8 \left(\frac{\rho}{M_G}\right) n_c \left(\frac{E_v}{E_1^{\mathrm{C-H}}}\right)_{\mathrm{C-X}} \tag{12}$$

where $D_{\max}$ is the attenuation in dB/km of the vth overtone of the C-X bond, ρ is the density of absorbing species in g/cm^3, M_G is the molecular weight of a repeat unit in g/mol, n_c is the number of the bonds of interest in the repeat unit and the ratio $E_v/E_1^{\mathrm{C-H}}$ is the overtone intensity related to the C-H fundamental. Therefore, in the Morse Potential calculation for the C-H bond of PMMA, the 6th harmonic vibration appears at 627-nm wavelength, which corresponds to the absorption loss of 427 dB/km. On the other hand, the 8th harmonic absorption loss of C-D bond appearing at almost the same wavelength (626 nm) for deuterated PMMA is about 0.82 dB/km which is about 520 times smaller than that of the 6th harmonic C-H absorption. However, even for the C-D bond, when the wavelength is longer than 1000 nm, the absorption loss becomes serious. For instance, the calculation loss due to the 4th harmonic vibration of C-D at 1174-nm wavelength is as large as 3670 dB/km. It was also recognized that [33] all-deuterated PMMA base POF had an absorption peak of O-H bond due to the slightly absorbed water molecules in the polymer.

On the other hand, it is well known that a fluoropolymer has very low water absorption. Furthermore, since the wavelength of the fundamental vibration of C-F bond is much longer than that of a C-D bond as mentioned above, the absorption loss even at 1171-nm wavelength, due to the 7th harmonic C-F vibration for an imaginary fluorinated PMMA, is still as low as 0.12 dB/km. Fluoropolymer must be an ultimate material for fabrication of the low-loss polymer optical fiber in near IR and IR regions.

Fig. 13 shows the total attenuation spectra of the MMA-d8 base and partially fluorinated acrylate base [34], [35] GI POF's compared with those of MMA-base GI POF. The minimum attenuation was summarized in Table III with the wavelength. The large absorption peak (2885 dB/km) of the MMA-base GI POF (curve C) exists at 735-nm wavelength due to the fifth harmonic generation of the C-H stretching vibration. On the other hand, the absorption peak of the partially fluorinated polymer-base GI POF is reduced to 815 dB/km because eight hydrogens in one monomer unit of PMMA is reduced to three hydrogens in the fluorinated acrylate [35]. In the PMMA-d8 base GI POF, there is no peak due to the C-H absorption. Since system components in near IR to IR regions such as light source, detector, and the environmental circuits have been already developed, such low loss POF even at such a wavelength is applicable for the current system.

C. Light Scattering Loss

In order to measure the light scattering loss and investigate the heterogeneities inside the preform rod, polarized (V_v) and depolarized (H_v) light scattering intensities by He-Ne laser (633 nm-wavelength) were measured against the scattering angle θ. Here, the GI preform rod was used as the sample

TABLE III
TOTAL ATTENUATION OF THE GI POF

	570 nm (dB/km)	650 nm (dB/km)	780 nm (dB/km)	Minimum (dB/km)
MMA-BB	90	113	840.5	90 (572 nm)
MMA-BBP	167	132	780	132(652 nm)
MMA-BEN	108	131	780	129(573 nm)
PMMA-d8 base	128	65.7	94	56 (688 nm)
Fuluoroacrylate polymer base	-	247	135	115 (774 nm)

for measurement. The measurement method is described as follows: the preform was placed vertically at the center of the goniometer and a He-Ne laser beam was injected from the side, and the scattered light from the center region of the rod was detected. The V_v and H_v light scattering intensities were measured, the details of which were described in our previous paper [36], [37]. Fig. 14 shows the experimental results of H_v and V_v scattering intensities against the scattering angle for the MMA-vinyl benzoate (VB) copolymer base GI preform we previously reported [38] and MMA-BEN base GI preforms. The H_v intensities for both GI preforms were independent of scattering angle and were c.a. 10^{-6}–10^{-7} cm^{-1}, which means that no anisotropic structures such as micro crystal and folded chain exist. On the other hand, the V_v scattering intensity for the MMA-VB copolymer base GI preform strongly increased with the decrease in the scattering angle and was in the range of 10^{-5} cm^{-1}. The V_v intensity for the MMA-BEN base GI preform is almost independent of the scattering angle and was in the range of 10^{-6} cm^{-1}. This V_v scattering measurement revealed that the copolymer base GI preform has some large size isotropic heterogeneities inside the matrix, while the MMA-BEN base GI preform has no such heterogeneities. To more quantitatively investigate the heterogeneities in the GI preform and estimate the effect of the scattering loss on the total attenuation of the GI POF, the scattering intensity measurement results were analyzed by the following procedure.

In randomly oriented polymer bulks, the isotropic part V_v^{iso} of the V_v is given by (13), [36], [37].

$$V_v^{\text{iso}} = V_v - (4/3)H_v. \tag{13}$$

Therefore, the observed V_v scattering was divided into three terms, $V_{v_1}^{\text{iso}}, V_{v_2}^{\text{iso}}$, and $(4/3)H_v$, as follows

$$V_v = (V_{v_1}^{\text{iso}} + V_{v_2}^{\text{iso}}) + (4/3)H_v \tag{14}$$

where the $V_{v_1}^{\text{iso}}$ denotes the isotropic background scattering independent of the scattering angle and the $V_{v_2}^{\text{iso}}$ is the isotropic scattering which depends on the scattering angle due to large size heterogeneities. Finally, the total scattering loss α_t (dB/km) is obtained by (15).

$$\alpha_t = 1.346 \times 10^6 \int_0^{\pi} \left\{ (1+\cos^2\theta)(V_{v1}^{\text{iso}} + V_{v2}^{\text{iso}}) + (13+\cos^2\theta) \times \frac{H_v}{3} \right\} \sin\theta \, d\theta. \tag{15}$$

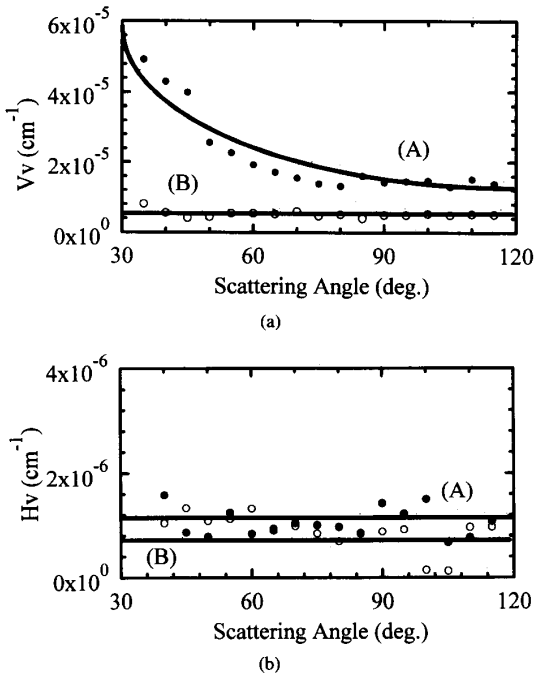

Fig. 14. (a) V_v and (b) H_v scattering intensities from the MMA-VB copolymer base and MMA-BEN base GI preforms. (A) MMA-VB copolymer base GI preform (•), (B) MMA-BEN based GI preform (○).

Here α_t is divided into three terms α_1^{iso}, α_2^{iso}, and α^{aniso}. That is

$$\alpha_t = \alpha_1^{\text{iso}} + \alpha_2^{\text{iso}} + \alpha^{\text{aniso}} \tag{16}$$

where, α_1^{iso} is the isotropic scattering loss from $V_{v_1}^{\text{iso}}$ with no angular dependence, α_2^{iso} is the isotropic scattering loss from $V_{v_2}^{\text{iso}}$ due to large-sized heterogeneities, and α^{aniso} is the anisotropic scattering from H_v.

Since the angular independence of H_v in Fig. 14 showed the random orientation, Debye's theory [39] written as (17) may be adopted

$$V_{v_2}^{\text{iso}} = \frac{4\langle\eta^2\rangle\pi^3}{\lambda_0^4} \int_0^{\infty} \frac{\sin(\nu s r)}{\nu s r} r^2 \gamma(r)\, dr \tag{17}$$

with

$$\nu = \frac{2\pi}{\lambda} \qquad s = 2\sin\left(\frac{\theta}{2}\right).$$

Here, $\langle\eta^2\rangle$ denotes the mean-square average of the fluctuation of all dielectric constants, λ_0 is the wavelength of light in vacuum and n is the refractive index of the sample. $\gamma(r)$ refers to the correlation function defined by

$$\gamma(r) = \langle\eta(r_i)\cdot\eta(r_j)\rangle_r / \langle\eta^2\rangle \tag{18}$$

where $\eta(r_i)$ and $\eta(r_j)$ are the fluctuations of dielectric constant at i and j positions which are a distance r apart. In this paper, the correlation function $\gamma(r)$ is assumed to be approximated by (18) as suggested by Debye *et al.* [39]

$$\gamma(r) = \exp\left(-\frac{r}{a}\right) \tag{19}$$

where a is called correlation length and is a measure of the size of the heterogeneities. Substituting (19) into (17) and

TABLE IV
SCATTERING PARAMETER OF THE GI PREFORMS AT 633 nm

	a (Å)	$\langle\eta^2\rangle$ ($\times 10^{-8}$)	α_1^{iso} (dB/km)	α_2^{iso} (dB/km)	α^{aniso} (dB/km)	α_t (dB/km)
MMA-BEN	0	0	10.35	0	9.46	19.81
MMA-co-VB*	762	0.74	6.1	33.9	10.1	50.4

integrating gives

$$V_{v_2}^{iso} = \frac{8\pi^3\langle\eta^2\rangle a^3}{\lambda_0^4(1+\nu^2 s^2 a^2)^2}. \tag{20}$$

The rearrangement of (20) gives the Debye plot [39], where $(V_{v_2}^{iso})^{1/2}$ versus s^2 shows a straight line, and correlation length a can be determined by $a = (\lambda/2\pi)$ (slope/intercept)$^{1/2}$.

The scattering parameters by above analysis are listed in Table IV. The α_1^{iso} corresponds to the intrinsic scattering loss caused by so called "thermal induced fluctuation," [37] and is written by

$$\alpha_1^{iso} = \left(\frac{80\log e}{27}\right)\frac{\pi^3}{\lambda_0^4}(n^2-1)^2(n^2+2)^2 kT\beta \tag{21}$$

where n is the refractive index of the polymer, k Boltzmann's constant, T the absolute temperature, β the isothermal compressibility, and λ_0 the wavelength of light in vacuum. Since the thermally induced fluctuation may be less than 50 Å in size which is much smaller than the correlation length a of the large size heterogeneities, the $V_{v_1}^{iso}$ intensity has no angular dependence. For instance, with using the published value of β [37], the α_1^{iso} of the PMMA estimated by (21) becomes less than 10 dB/km. On the other hand, the scattering loss α_2^{iso} of approximately 34 dB/km in the MMA-vinyl benzoate (VB) copolymer base GI POF is caused by the heterogeneities with the correlation length a of 700 Å and $\langle\eta^2\rangle$ of 7.4×10^{-9}. If it is assumed that these heterogeneities consist of two phases in which each volume fraction is ϕ_A and ϕ_B, and the refractive indices are n_A and n_B, respectively, the a and $\langle\eta^2\rangle$ are given by [36], [37]

$$a = \frac{4V}{S}\phi_A\phi_B \tag{22}$$

$$\langle\eta^2\rangle \cong \phi_A\phi_B(n_A-n_B)^2 \cong 4\phi_A\phi_B n^2(\Delta n) \tag{23}$$

where S is the total surface area of the boundary between the two phases, V is the total volume, n is the average refractive index, and Δn is $(n_A - n_B)$, and $\phi_A + \phi_B = 1$. Equation (22) indicates that if the boundary surface of the two phases are intricate each other, the value of S increases to give a smaller value of the correlation length. Equation (23) shows that if $\phi_A = 0.1$-0.9, the fluctuation of the refractive index (the difference of the refractive indices between n_A and n_B, Δn) is in the order of 10^{-5}.

As the origin of these heterogeneities inside the MMA-VB copolymer base GI preform, we should also investigate the effect of the distribution of the copolymer composition from the monomer reactivity ratio, r_1 and r_2 [40]. Those calculation methods are described elsewhere [41].

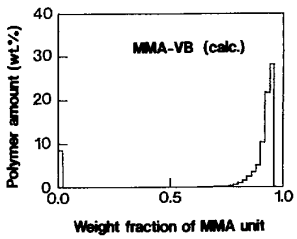

Fig. 15. Calculated distribution of copolymer composition after 100% polymerization when MMA/VB = 4/1 (wt./wt.).

The histogram when calculated in the MMA-VB copolymer base at MMA/VB = 4/1 (wt./wt.) is shown in Fig. 15, which corresponds to the copolymer composition after completing polymerization. Here, VB monomer was one of the suitable monomers to form the copolymer base GI preform by our previous technique utilizing the monomer reactivity [41]. In the case of MMA-VB copolymers, the monomer reactivity ratios are $r_1 = 8.52$, r_2 = 0.07, which means that the MMA monomer is much more reactive than the VB monomer since $r_1 \gg 1$ and $r_2 \ll 1$. (In the case of random copolymerization, $r_1 \approx r_2 \approx 1.0$.) Therefore, the MMA monomer is preferentially polymerized at the initial stage of the copolymerization and is almost completely consumed during the copolymerization. After that, the homopolymer of VB is formed. Namely, distribution of the copolymer composition is mainly divided into two compositions: one is formed at the initial stage of polymerization and is quite similar to that of PMMA, and the other formed at the final stage of polymerization and is almost VB homopolymer as shown in Fig. 15. Therefore, we can say that the composition of the poly (MMA-VB) is similar to blend polymer. This calculation result may imply that the excess scattering loss α_2^{iso} of 34 dB/km in Table IV is caused by the large size (a = 760 AA) heterogeneities due to the semi-blend structure as shown in Fig. 15.

On the other hand, in the case of the MMA-BEN system preform, no large-sized heterogeneities were recognized because $\alpha_2^{iso} = 0$, which means that each BEN dopant molecule is randomly located without any aggregation causing the large heterogeneous structures. Almost the same solubility parameters of 9.3 $(cal/cm^3)^{1/2}$ and 9.6 $(cal/cm^3)^{1/2}$ for PMMA and BEN molecule, respectively, in Table II means that the BEN molecule is quite miscible in the PMMA matrix which also supports the result of $\alpha_2^{iso} = 0$ in Table IV. Therefore, it is concluded that regarding the scattering loss, the new GI POF based on the MMA-M_2 unreactive dopant base is superior to the previous copolymer base GI POF utilizing the difference of monomer reactivity.

VI. 2.5 Gb/s DIGITAL DATA TRANSMISSION FOR 100 m GI POF

Data transmission experiment was carried out by using the edge emitting red LD with 647 nm wavelength which was newly developed by NEC Co. Ltd. for high-speed data transmission [42]. In the conventional optical transmission system, the LD with 1.3 μm wavelength was used. However, it

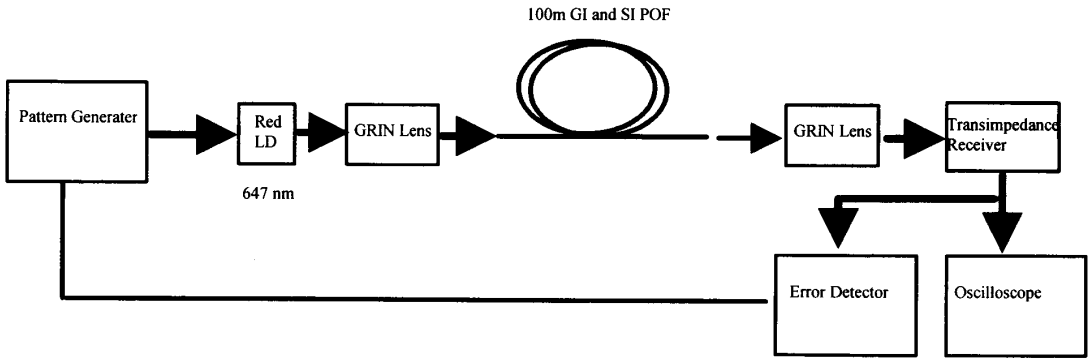

Fig. 16. A block diagram of a 2.5 Gb/s, 100 m POF link.

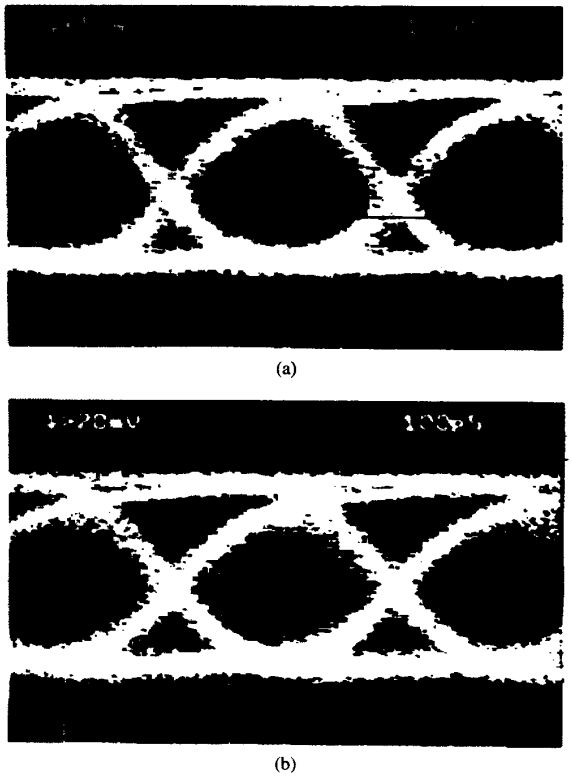

(a)

(b)

Fig. 17. Received waveform at 2.5 Gb/s. (a) Back to back, (b) after 100 m GI POF.

should be difficult to use the same system component for POF systems because of the excessive attenuation at the near infrared region as mentioned above. Therefore, the development of the high-speed red LD whose emission wavelength is the same as the optical window (around 650 nm wavelength) of the PMMA base POF enabled the breakthrough for high-speed POF network system. Without any speed up circuit, the LD can be modulated up to 2.5 Gb/s, which is also great advantage in the aspect for the total system cost. The block diagram of the system component is shown in Fig. 16. A 2.5 Gb/s, $2^{15}-1$, NRZ PN pattern was passed to the laser. The laser output was coupled into a POF with a GRIN rod lens. Fiber launched power was +6.1 dBm at maximum. After 100 m light transmission, the optical signal was attenuated by 20 dB due to the fiber attenuation. The fiber output signal was coupled into the Si PIN PD with a 400 μm diameter, via a GRIN rod lens. A PIN FET optical receiver was used. Fig. 17(a) and (b) show the eye diagram before and after 2.5 Gb/s 100 m length transmission. In order to compare the effect of fiber bandwidth on the waveform, the performance of the commercially available SI POF was investigated. The launched NA was set to 0.2 to decrease the effect of the modal dispersion. Fig. 18 shows the eye diagram after 250 Mb/s, 100 m signal transmission using the SI POF. Walker *et al.* reported [43] the possibility to transmit 1 Gb/s over 100 m in the SI POF link by using the equalizer at the receiver in order to compensate the mode partition noise. However, without such equalization, the modal dispersion of the SI POF caused too severe the eye closure even at 250 Mb/s of bit rate. Fig. 19 shows the plots of the measured bit error rate versus received average power at 2.5 Gb/s of bit rate with and without using the 100 m-length GI POF. Receiver sensitivity was -16.9 dBm at 10^{-9} bit error rate. Error rate characteristics for the GI POF were almost the same as those back-to-back transmission, and a 0.6 dB receiver sensitivity degradation was observed after 100 m signal transmission. This power penalty is attributed to the effect of modal dispersion in the GI POF, because the theoretical limitation of the signal rate attributed to the material dispersion of PMMA was calculated to be approximately 3 Gb/s.

VII. Mechanical Properties

Considering the use of POF's for data communication, some mechanical properties such as tensile strength and thermal resistance are also required. In the new GI POF, since the M_2 molecules are doped, we have to investigate the thermal resistance for migration of the dopant. The stability of the index-profile of this GI POF at 85°C was evaluated. Fig. 20 shows the experimental result of the thermal resistance of refractive-index profile of the MMA-BEN GI POF. The curve (b) in Fig. 20 is the index profile measured after heat-treatment at 85°C for 2 weeks, while the curve (A) is the index-profile of the original fiber. It was experimentally confirmed that the refractive-index profile did not change at 85°C for 2 weeks.

TABLE V
MECHANICAL PROPERTIES OF THE GI POF

POF	Heat-drawing temperature (°C)	Yield Strength (kgf/cm²)	Tensile Strength (kgf/cm²)	elongation (%)
MMA-BzMA	190	1060	1620	33
MMA-BzMA	250	712	634	9
MMA-VB	190	737	683	7
MMA-BB	175	-	2050	39
MMA-BB	195	1170	1340	34
MMA-BBP	190	1260	1880	43
MMA-BBP	195	960	970	51
MMA-BEN	200	1052	1092	36
SI	-	970	1040	67

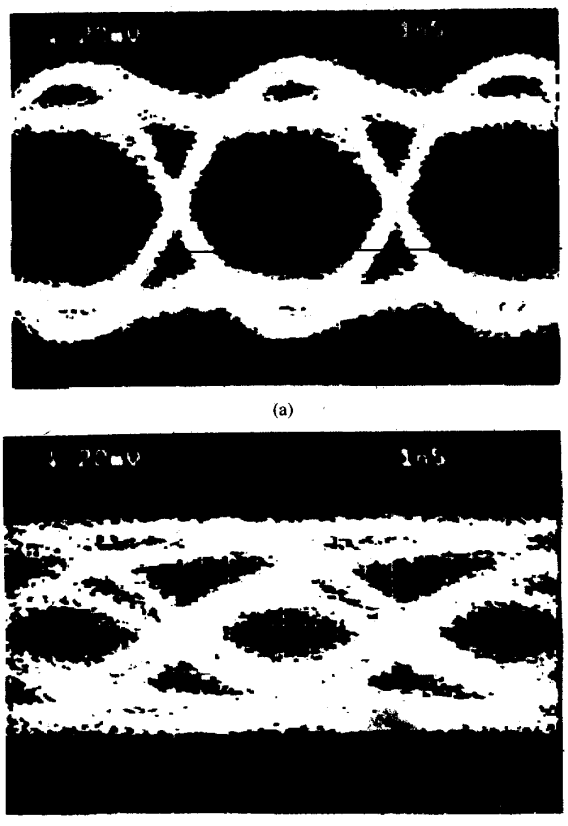

(a)

(b)

Fig. 18. Received waveform at 250 Mb/s. (a) Back to back, (b) after 100 m SI POF.

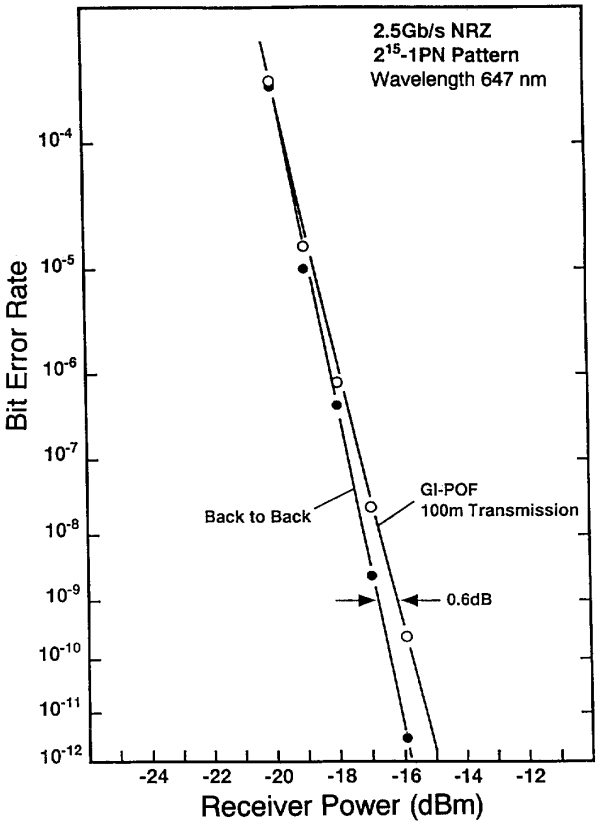

Fig. 19. Measured bit error rate for 2.5 Gb/s 100 m GI POF link.

The tensile strength measurement results are shown in Table V. The yield strength and the tensile strength of the MMA-dopant system GI POF's (950–2000 kg/cm^2) are almost the same as or superior to those of commercially available SI POF (1000 kg/cm^2), while the elongation of the GI POF's (about 30–50%) is a little lower than that of SI POF (60%). However, these total mechanical properties may be sufficient for practical use.

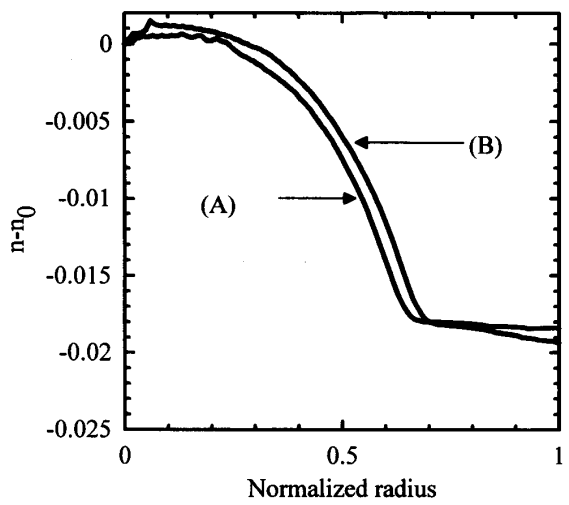

Fig. 20. Thermal stability of the refractive-index profile of MMA-BEN system GI POF for 2-weeks at 85°C. (A) Room Temperature. (B) 85°C.

VIII. System Application

Not only in the network termination (NT) area of fiber to the home (FTTH) but many application fields in which the GI POF can be applicable are considered. For instance, in the popular satellite cable television system, the signal from the converter to the tuner is transmitted by the coax cable to cover the high frequency which is about 1 GHz. As the promising alternative, the GI POF might be preferable because of several advantages of optical fiber. With the extent of subscriber in cable television (CATV) network, multichannels and clear vision TV also became popular. The GI POF can play the role in the area of less than 200 m transmission distance, namely in a building and home. For such a CATV system and interactive communication network, Domestic Passive Optical Network (DPON) concept was proposed from Philips [44], and it was modified by applying the high bandwidth GI POF from the network termination to each room, which are shown in Figs. 21 and 22. As the media for indoor use, at first, metallic cables such as coax and twisted pair were considered because of easy installation and inexpensive cost as shown in Fig. 21. However, in the modified proposal shown in Fig. 22, the single mode fiber was used in the trunk area, while the use of GI POF was also achieved by alternating the used wavelength from 1.3 $\sim$ 1.55 μm to 650 nm or 780 nm in an Optical-Electrical transducer as proposed from Fujitsu. Co. [11].

Regarding the cost of the GI POF, the fabrication method of the GI POF is very simple as mentioned in Section III, "Preparation of GI POF," and used materials such as MMA monomer and dopants in this process are basically inexpensive. Since the GI POF is still at the laboratory stage, it is difficult to predict the cost if the GI POF is commercially available. However, we have not noticed serious cost-increasing factors compared with the commercially available SI POF, the price of the GI POF may be much less expensive than that of silica based optical fiber.

Other several application fields suitable for the POF and metallic cables are summarized in Fig. 23 with a data rate

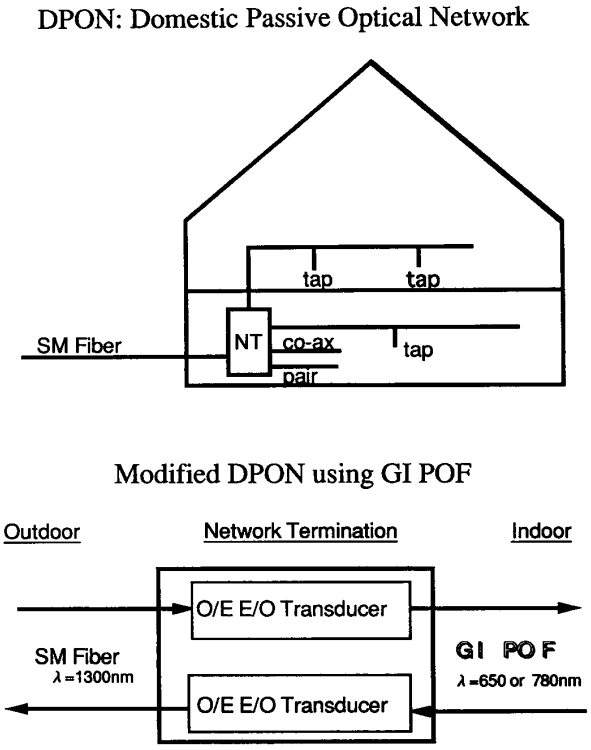

Fig. 21. Schematic representation of domestic passive optical network (DPON) concept proposed from Philips.

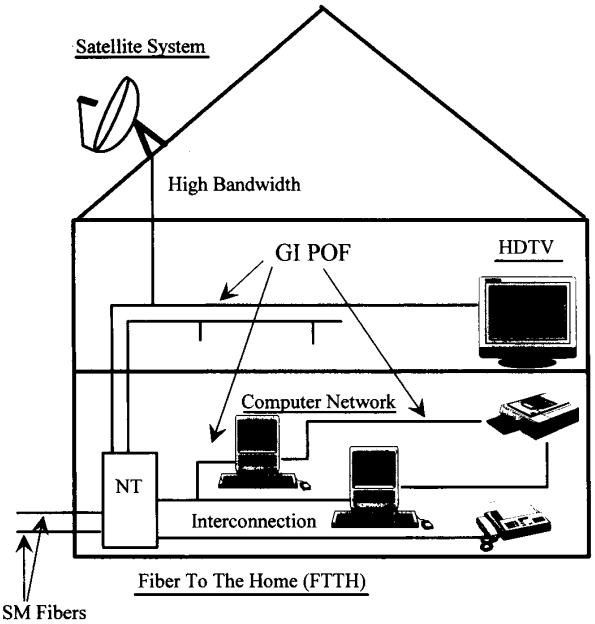

Fig. 22. Schematic representation of the high-speed multimedia network concept using the large core high bandwidth GI POF.

and transmission distance relationship. The conventional inexpensive metallic cables such as twist-pair and coax cables are compared with the POF's. In general, possible data rate through the conventional metallic cable is less than 100 Mb/s

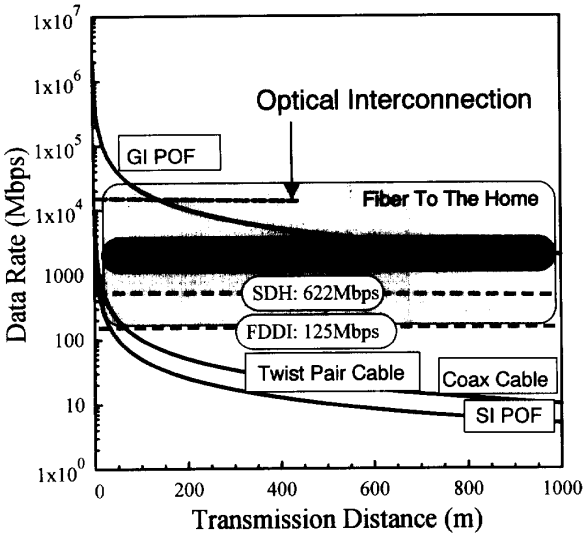

Fig. 23. Relationship between data rate and the application fields of several media.

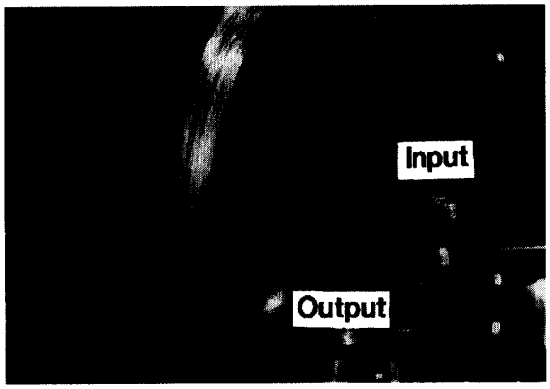

Fig. 24. Demonstration of light transmission through 200-m length MMA-BEN system GI POF by using 1.5 mW laser diode at 652-nm wavelength.

except for the high bandwidth coax cable. On the other hand, the GI POF is considered to work well in required high-speed data rate for FDDI or SDH standards, while the conventional SI POF cannot cover such a data rate.

The large problem for the high-speed POF network lies in the data rate of light source. In the case of the low rate (less than 10 Mb/s) transmission standard such as the TOSLINK (registered trade name of Toshiba Co.), high power visible light emitting diode (LED) suitable for the SI POF's optical window can be adopted. On the other hand, when using the GI POF the total signal rate is seriously restricted by a large spectrum width and large rise and fall time of the LED. Therefore, a visible laser diode (LD) with a high speed and narrow spectrum must be developed. A red vertical cavity surface emitting laser (VCSEL) reported by Schneider *et al.* is very attractive for GI POF link because it was successfully operated at 622.08 Mb/s [45] of data rate.

The compact disk laser diode operated at 780-nm wavelength is also one of the candidates suitable for high-speed POF system. The advantage of the compact disk laser goes beyond the cost. The first rise and fall time of GaAlAs lasers provide optical link data rates up to 1 Gb/s [46]. Note that the attenuation of the conventional MMA-base POF is more than 500 dB/km at this wavelength which will limit the transmission distance within 10 to 20 m. Therefore, the low absorption loss POF at near infrared region, such as all deuterated MMA-base or fluorinated polymer base as mentioned above, is required.

Fig. 24 shows the photograph of the demonstration of light transmission through the GI POF. As the light source, a laser diode whose emission peak is located at 655-nm of wavelength and whose emission power is 1.5 mW was used. The fiber length was 200-m.

IX. Conclusion

A high-bandwidth (2 GHz · km) GI POF with good mechanical properties was successfully obtained by the interfacial-gel polymerization technique. The attenuation of transmission was 90 dB/km at 572-nm wavelength for PMMA base GI POF and was 56 dB/km at 688-nm wavelength for the all deuterated PMMA base GI POF, which is enough to cover short distance communication such as in a building or home. The new GI POF based on the MMA-M_2 unreactive dopant system is superior to the previous copolymer base GI POF in the attenuation of transmission, because no large heterogeneities exists in the new GI POF.

Although the PMMA base GI POF has large attenuation as 800 dB/km at 780-nm wavelength due to carbon-hydrogen stretching vibration, in which inexpensive laser diode has been commercially available, all deuterated PMMA base and partially fluoroacrylate base GI POF's provided low attenuation as about 100 dB/km at the same wavelength. Since all the current data transmission systems have been of near IR and IR use, such low loss GI POF's at near IR regions is very practical for the system application.

The short rage data communication systems such as FDDI were currently provided much more economically by using metallic cables instead of the standard fiber, because of the cost of connector. With increasing the data rate up to several hundred Mb/s (ex. SDH standard), the termination area of the metallic cable network also becomes expensive, since very complicated modulation is required. The large core GI POF which enables easy connection with very low cost connector fabricated by the injection molding may decrease the total cost of the system. Furthermore, the bandwidth of the GI POF was the order of GHz · km which is sufficient to cover the required signal rate.

The high bandwidth GI polymer optical fiber will open the way towards the low-cost and high-speed multimedia network architecture.

Acknowledgment

The authors wish to acknowledge Dr. C. E. Forbes, Dr. L. LaNieve, Dr. R. Straff, Dr. A. Tanaka, Dr. S. Yamazaki, and Dr. G. D. Khoe for valuable discussion and cooperation.

REFERENCES

[1] C. Emslie, "Review polymer optical fibres," *J. Mat. Sci.*, vol. 23, pp. 2281–2293, 1988.

[2] W. Groh, D. Lupo, and H. Sixl, "Polymer optical fibers and nonlinear optical device principles" *Angew. Chem. Int. Ed. Engl. Adv. Mater.*, vol. 28, no. 11, pp. 1548–1559, 1989.

[3] T. Ishigure, E. Nihei, and Y. Koike, "Graded-index polymer optical fiber for high-speed data communication," *Appl. Opt.*, vol. 33, no. 19, pp. 4261–4266, 1994.

[4] Plastic Optical Fibers and Applications Conference, in *EFOC/LAN POF '92*, Paris, June 1992.

[5] ——, in *POF '93*, Den Hague, June 1993.

[6] —— *Proc. SPIE*, Vol. 1592, Boston, Sept. 1991.

[7] "Plastic optical fibers," *Proc. SPIE*, Vol. 1799, Boston, Sept. 1993.

[8] J. Meier, W. Lieber, W. Heinlein, and W. Groh, "Time-domain bandwidth measurement of step-index plastic fibres," *Electron. Lett.*, vol. 22, pp. 1208–1209, 1987.

[9] ANSI X3T9.5 draft FDDI physical layer medium dependent standard, Rev. 8.0, July 1, 1990.

[10] *CCITT Blue Book*, Recommendations G. 707, G. 708, and G. 709, 1989.

[11] A. Tanaka, "Application of plastic optical fiber to data communications," in *Proc. MIYAZAKI Int. Symp. Optical and Electrical Properties of Organic Materials*, Proc. B-23-25, Tokyo, June 1992.

[12] Y. Koike, "High bandwidth, low loss polymer fibers," in *Proc. ECOC '92*, Vol. 2, 1992, pp. 679–686.

[13] T. Kaino, *Polymers for Lightwave and Integrated Optics*. New York: Marcel Dekker, 1992, ch. 1, pp. 1–38.

[14] M. Kitazawa, *POF Data Book*, MRC Techno, Inc., Tokyo, 1993.

[15] M. H. Schleinitz, "Ductile plastic optical fibers with improved visible and near infrared transmission," in *Proc. Int. Wire Cable Symp.*, vol. 26, 1977, pp. 352–355.

[16] T. Kaino, M. Fujiki, S. Oikawa, and S. Nara, "Low-loss plastic optical fibers," *Appl. Opt.*, vol. 20, pp. 2886–2888, 1981.

[17] S. Oikawa, M. Fujiki, and Y. Katayama, "Plastic optical fiber with improved transmitance," *Electron. Lett.*, vol. 15, pp. 829–830, 1979.

[18] T. Kaino, M. Fujiki, and K. Jinguji, "Preparation of plastic optical fibers," *Rev. Electron. Commun. Lab.*, vol. 32, pp. 478–488, 1984.

[19] Mitsubishi Rayon Co., U.K. Patent 1431157, 1974.

[20] T. Kaino, K. Jinguji, and S. Nara, "Low-loss poly(methyl methacrylate-d8) core optical fibers," *Appl. Phys. Lett.*, vol. 42, pp. 567–569, 1983.

[21] Y. Koike, Y. Kimoto, and Y. Ohtsuka, "Studies on the light-focusing plastic rod. 12: The GRIN fiber lens of methyl methacrylate-vinyl phenyl acetate copolymer," *Appl. Opt.*, vol. 21, pp. 1057–1062, 1982.

[22] Y. Ohtsuka and Y. Koike, "Studies on the light-focusing plastic rod. 18: Control of refractive-index distribution of plastic radial gradient-index by photocopolymerization," *Appl. Opt.*, vol. 24, pp. 4316–4320, 1985.

[23] J. C. Palais, "Fiber coupling using graded-index rod lenses," *Appl. Opt.*, vol. 19, pp. 2011–2018, 1980.

[24] *Rodscope*, Mitsubishi Rayon Co. Ltd., Japan.

[25] Y. Koike, *Polymers for Lightwave and Integrated Optics*. New York, Marcel Dekker, 1992, ch. 3, pp. 71–104.

[26] A. D. Pearson, W. G. French, and E. G. Rawson, "Preparation of a light focusing glass rod by ion-exchange techniques," *Appl. Phys. Lett.*, vol. 15, no. 2, p. 76, 1969.

[27] H. Kita. I. Kitano, T. Uchida, and M. Furukawa, "Light-focusing glass fibers and rods," *J. Am. Cer. Soc.*, vol. 54, no. 7, pp. 321–326, 1971.

[28] S. Takahashi and K. Ichimura, "Time domain measurements of launching-condition-dependent bandwidth of all-plastic optical fibres," *Electron. Lett.*, vol. 27, pp. 217–220, 1991.

[29] R. Olshansky and D. B. Keck, "Pulse broadening in graded-index optical fibers," *Appl. Opt.*, vol. 15, pp. 483–491, 1976.

[30] D. Gloge and E. A. J. Marcatili, "Multi mode theory of graded-core fibers," *Bell Syst. Tech. J.*, vol. 52, pp. 1563–1578, 1973.

[31] F. Urbach, "The long-wavelength edge of photographic sensitivity and of the electronic absorption of solids," *Phys. Rev.*, vol. 92, pp. 1324–1325, 1953.

[32] W. Groh, "Overtone absorption in macromolecules for polymer optical fibers," *Makromol. Chem.*, vol. 189, pp. 2861–2874, 1988.

[33] P. Avakian, W. Y. Hsu, P. Meakin, and H. L. Snyder, "Optical absorption of perdeuterated PMMA and influence of water," *J. Polym. Sci. Polym. Phys. Ed.*, vol. 22, pp. 1607–1613, 1984.

[34] H. A. Deckers, T. Dittmer, R. W. Fuss, and R. Strern, "Application of fluoropolymers in optical fibres," in *Proc. Fluoropolymer Conf.*, Manchester, Jan. 1992, Paper 12, pp. 1–6.

[35] T. Ishigure, E. Nihei, Y. Koike, C. E. Forbes, L. LaNieve, R. Straff, and H.A. Deckers, "Large-core, high-bandwidth polymer optical fiber for near infrared use," *IEEE Photon. Tehnol. Lett.*, vol. 7, pp. 403–405, 1995.

[36] Y. Koike, N. Tanio, and Y. Ohtsuka, "Light scattering and heterogeneities in low-loss poly(methyl methacrylate) glasses," *Macromolecules*, vol. 22, pp. 1367–1373, 1989.

[37] Y. Koike, S. Matsuoka, and H. E. Bair, "Origin of excess light scattering in poly(methyl methacrylate) glasses," *Macromolecules*, vol. 25, pp. 4809–4815, 1992.

[38] Y. Koike and Y. Ohtsuka, "Low-loss GI plastic fiber and novel optical polymers," *Mat. Res. Soc. Symp. Proc.*, vol. 172, pp. 247–252, 1990.

[39] P. Debye, H. R. Anderson, and H. Brumberger, "Scattering by an inhomogeneous solid. II. The correlation function and its application," *J. Appl. Phys.*, vol. 28, pp. 679–683, 1957.

[40] J. Brandrup and E. H. Immergut, *Polymer Handbook*, second edition. New York: Wiley, 1975.

[41] Y. Koike, "High-bandwidth graded-index polymer optical fibre," *Polymer*, vol. 32, pp. 1737–1745, 1991.

[42] T. Ishigure, E. Nihei, S. Yamazaki, K. Kobayashi, and Y. Koike, "2.5 Gb/100 m data transmission using graded index polymer optical fiber and high speed laser diode at 650-nm wavelength," *Electron. Lett.*, vol. 31, pp. 467–468, 1995.

[43] S. D. Walker and R. J. S. Bates., "Towards gigabit plastic optical fibre data links: Present progress and future prospects," in *Proc. 2nd Int. Conf. Plastic Optical Fibre and Its Applications*, 1993, pp. 8–13.

[44] G. D. Khoe, J. H. Angenent, and J. T. Kluitmans, "DPON: Domestic passive optical network," in *Proc. ECOC '91*, 1991, pp. 737–740.

[45] D. M. Kuchta, F. J. Canora, R. P. Schneider Jr., J. A. Lott, and K. D. Choquette, "Performance of fiber optic data links using 570 nm cw VCSELs and a monolithic Si photodetector and CMOS preamplifier," in *Proc. Opt. Fiber Conf.*, San Jose, Feb. 1994.

[46] M. J. Heckert, "Performance of telecommunication-grade multimode fiber at 780 nm," *J. Lightwave Technol.*, vol. 10, pp. 712–719, 1992.

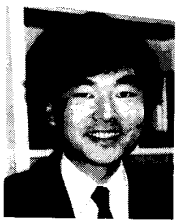

Yasuhiro Koike was born in Japan on April 7, 1954. He received the B.S., M.S. and Ph.D. degrees from Keio University, Japan, in 1977, 1979, and 1982, respectively.

He has been an Associate Professor at Keio University and developed the high bandwidth GI polymer optical fiber. He was a Visiting Researcher at AT&T Bell Laboratories from 1989 to 1990.

Dr. Koike received the International Engineering and Technology Award of the Society of Plastics Engineers in 1994.

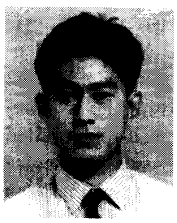

Takaaki Ishigure was born in Gifu, Japan on July 30, 1968. He received the B.S. degree in applied chemistry and the M.S. degree in material science from Keio University in 1990 and 1992, respectively.

He is in the Ph.D. degree program at Keio University. His current research interests are in the fabrication and system application of the graded index polymer optical fiber.

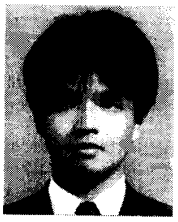

Eisuke Nihei was born in Fukushima, Japan, on October 17, 1962. He received the B.S. degree in applied chemistry in 1985 and the Ph.D. degree in material science from Keio University, researching high-bandwidth low-loss graded index polymer optical fiber in 1990.

He worked at Keio University where he is an Instructor. His current research interests are about photonics polymer.